small NANO MICRO

Drug delivery

Magnetic Luminescent Porous Silicon Microparticles for Localized Delivery of Molecular Drug Payloads

*Luo Gu, Ji-Ho Park, Kim H. Duong, Erkki Ruoslahti, and Michael J. Sailor**

***M**agnetic manipulation, fluorescent tracking, and localized delivery of a drug payload to cancer cells in vitro is demonstrated, using nanostructured porous silicon microparticles as a carrier. The multifunctional microparticles are prepared by electrochemical porosification of a silicon wafer in a hydrofluoric acid-containing electrolyte, followed by removal and fracture of the porous layer into particles using ultrasound. The intrinsically luminescent particles are loaded with superparamagnetic iron oxide nanoparticles and the anti-cancer drug doxorubicin. The drug-containing particles are delivered to human cervical cancer (HeLa) cells in vitro, under the guidance of a magnetic field. The high concentration of particles in the proximity of the magnetic field results in a high concentration of drug being released in that region of the Petri dish, and localized cell death is confirmed by cellular viability assay (Calcein AM).*

1. Introduction

Multifunctional microparticles that are simultaneously magnetic and fluorescent have attracted interest because they can be manipulated with an external magnetic field while being tracked by fluorescence imaging in real time.[1–7] Several examples of potential uses have been demonstrated: immunoassays for bacterial spores or explosives,[8,9] cell-based or DNA assays,[10–13] gene expression profiling,[14] chemical sensing,[15] and safety controls of medical devices.[16] Preparation of such multifunctional microparticles generally involves incorporating the fluorescent (organic fluorophore, quantum dot) and magnetic (iron oxide nanoparticle) components into a non-functional matrix like silica spheres or polystyrene beads.[1,2,7,13,17–19] Issues associated with this approach include quenching or leakage of the luminescent species,[6,12,17,18] as well as photobleaching (in the case of organic fluorophores).[20,21] Although quantum dots typically display greater stability than organic dyes, toxicity of heavy-metal-containing quantum dots[22] limits their use in many biological applications.

Intrinsically luminescent silicon nanostructures offer an alternative fluorophore that can be as photostable as the conventional II-VI quantum dots,[23–25] but with lower *in-vivo* or *in-vitro* toxicity.[24–29] Silicon is an essential trace element that is widely distributed in various mammalian (including human) tissues[30,31] in the form of orthosilicate (SiO_4^{4-}). Orthosilicate is the primary product of porous Si degradation in vitro and in vivo, and the low toxicity and biocompatibility of porous Si has been demonstrated.[32,33] Moreover, porous Si nanostructures can act as a host matrix for molecules, enzymes, proteins, magnetic nanoparticles, or other species.[34–37] In this work, magnetic luminescent Si microparticles with porous nanostructures are prepared by incorporating superparamagnetic iron oxide nanoparticles into the intrinsically luminescent porous Si matrix to provide a composite that is simultaneously fluorescent and magnetic. The anticancer drug doxorubicin is loaded into the dual-functional microparticles, and the drug is delivered to human cervical cancer (HeLa) cells *in vitro* under the guidance of a magnetic field, demonstrating magnetic manipulation, fluorescent tracking, and localized delivery of a molecular payload.

L. Gu, Dr. J.-H. Park, K. H. Duong, Prof. M. J. Sailor
Department of Chemistry and Biochemistry
Materials Science and Engineering Program
University of California
San Diego, 9500 Gilman, La Jolla, CA 92093, USA
E-mail: msailor@ucsd.edu
Prof. E. Ruoslahti
Burnham Institute for Medical Research at UCSB
University of California
Santa Barbara, 1105 Life Sciences Technology Bldg.
Santa Barbara, CA 93106, USA

DOI: 10.1002/smll.201000841

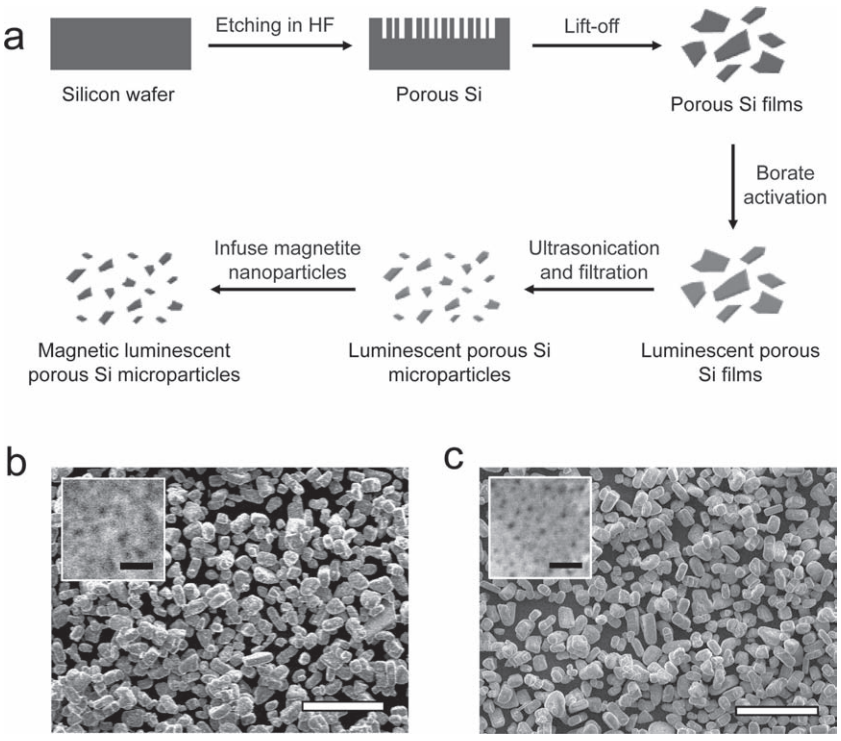

Figure 1. (a) Schematic depicting the synthesis of magnetic luminescent porous Si microparticles. A porous Si layer is first etched into a single-crystal Si wafer in ethanolic HF solution. The porous layer is removed from the substrate by application of a current pulse ("Lift-off"), and the freestanding porous Si fragments are then dispersed in a mild oxidant (aqueous borate) to activate photoluminescence. The luminescent fragments are then fractured into microparticles by ultrasonication. Finally, magnetite nanoparticles are loaded into the microparticles and locked into place by mild oxidation in air (100 °C). Scanning electron microscope (SEM) images of luminescent porous Si microparticles before (b) and after (c) loading of magnetite nanoparticles. Insets of both images reveal the porous nanostructures. Pore sizes before and after magnetite loading are 21 ± 4 nm and 12 ± 3 nm, respectively. The diameter of the magnetite nanoparticles used in this experiment is 13 ± 2 nm. The scale bars are 100 μm (100 nm for the insets).

2. Results and Discussion

Magnetic, luminescent porous Si microparticles were prepared as outlined in **Figure 1**a. Electrochemical etching of highly doped p-type single-crystal Si wafers in an aqueous HF solution containing ethanol produces a porous layer, which is removed from the Si substrate with a secondary current pulse. In order to activate photoluminescence, the porous Si layer is mildly oxidized in an aqueous borate buffer solution (pH = 9.2). The film is then fractured by ultrasonication and filtered to remove fragments <5 μm in size. Scanning electron microscopy (SEM) reveals uniform microparticles, with an average size of 19 ± 4 μm (n = 50, S.D.) and an average pore diameter of 21 ± 4 nm (Figure 1b). Fourier-transform infrared (FTIR) spectroscopy indicates that the oxidation step removes surface Si-H species from the material, generating a silicon oxide shell (Supporting Information, Figure S1).

The microparticles display a strong orange to near-IR photoluminescence (**Figure 2**a), which is attributed to quantum confinement effects in the silicon cores and to Si-SiO_2 interfacial defects generated during the activation step.[1,38,39] Nitrogen adsorption/desorption measurements reveal a type IV isotherm with a pronounced hysteresis loop, indicating the nanostructure of the microparticles is mesoporous (pore diameters 2–50 nm). The specific surface area (BET method) and pore volume (BJH method) are 520 $m^2\ g^{-1}$ and 0.712 $cm^3\ g^{-1}$, respectively (Supporting Information, Figure S2a).

Magnetic properties were imparted to the luminescent porous Si microparticles by infusion of iron oxide nanoparticles. Superparamagnetic Fe_3O_4 nanoparticles with mean diameters of 13 ± 2 nm (measured by transmission electron microscopy) were synthesized following a published method.[40] The nanoparticles were infused into the luminescent porous Si microparticles by placing the microparticles in an aqueous solution of iron oxide nanoparticles as described previously.[34,41] Once loaded, the microparticles were harvested from the suspension by centrifugation, and the iron oxide nanoparticles were trapped in the porous Si matrix by thermal oxidation/dehydration of the isolated particles in air at 100 °C for 8 h.

The luminescent microparticles retain their overall size upon infusion of iron oxide nanoparticles. However, the average pore diameter (12 ± 3 nm), surface area (373 $m^2\ g^{-1}$) and pore volume (0.577 $cm^3\ g^{-1}$) are reduced compared to the iron-free microparticles (Figure 1c and Supporting Information, Figure S2b). The intrinsic photoluminescence of the iron oxide-containing microparticles is similar to the iron-free microparticles, although a slight blue shift in the emission spectrum is consistently observed. This blue shift is attributed to a decrease in size of the emissive Si nanoparticles within the porous Si matrix, caused by the oxidation process (Figure 2a).[42] The magnetic composite materials exhibit similar photostability to other inorganic solid state nanoparticles. Like quantum dots deriving from II-VI compounds, the porous Si microparticles are significantly more photostable compared with fluorescent organic dye molecules, and they are resistant to photobleaching when exposed to UV light (Supporting Information, Figure S3). The quantity of iron oxide nanoparticles loaded in the porous Si microparticle carriers is 0.8% by weight (based on mass of Fe_3O_4, measured by inductively coupled plasma-optical emission spectrometry, ICP-OES). Superconducting quantum interference device (SQUID) data indicates that the magnetic nanoparticles retain their superparamagnetic characteristic when incorporated in the luminescent porous Si host, with a saturation magnetization value of 0.37 emu g^{-1} (based on mass of the composite microparticles, Figure 2b). Because the microparticles contain both magnetic and fluorescent functions, they can be manipulated with an

small NANO MICRO

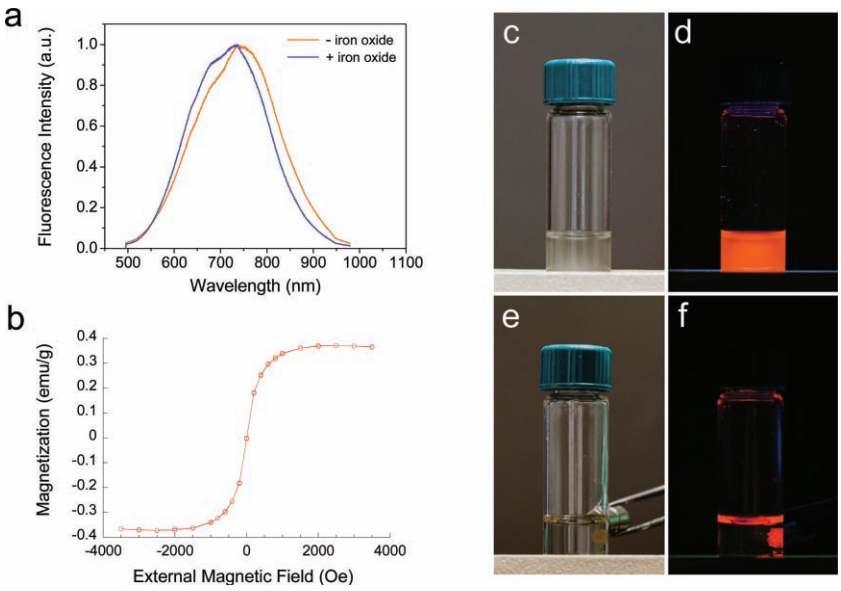

Figure 2. (a) Photoluminescence emission spectra of porous Si microparticles before and after loading of magnetite nanoparticles (excitation wavelength 370 nm). The intrinsic photoluminescence of the Si nanostructure is not significantly altered upon loading of iron oxide nanoparticles. (b) Room-temperature magnetization curve of porous Si microparticles loaded with iron oxide (magnetite) nanoparticles. Magnetization data are based on total mass of the composite microparticles. (c) Photograph of magnetic, luminescent microparticles suspended in water. (d) Corresponding image obtained under UV light. (e) The microparticles from (c) are attracted to a rare earth magnet and can be pinned to the side of the glass vial. (f) Corresponding image obtained under UV light. The appearance of orange color at the meniscus of the liquid is due to luminescence light emanating from the pinned particles refracting at the air/water interface.

external magnetic field and tracked by fluorescence imaging (Figure 2c–f).

As indicated by the BET data, the microparticles still possess free open volume after loading of the iron oxide nanoparticles. This potentially allows the incorporation of an additional payload. In this work, the anticancer drug doxorubicin (DOX) was loaded as a test molecule payload, using a simple adsorption protocol. The iron oxide containing porous Si microparticles were exposed to an aqueous solution of DOX for 1 h, and the particles were harvested from the solution with the aid of a rare earth permanent magnet. The DOX molecules are sufficiently strongly adsorbed that they are not readily removed by rinsing with pure water. However, the DOX molecules are slowly leached into a phosphate buffered saline solution over a period of several days (**Figure 3**c). Approximately 0.109 mg of DOX was loaded per milligram of magnetic luminescent porous Si microparticles (9.8% by mass). Based on the measured (BET) surface area, the theoretical percent loading of a monolayer of DOX, is 4.4%, which is significantly smaller than the experimental result. The larger loading of DOX measured experimentally represents multilayer adsorption, attributed to electrostatic interactions between the positively charged DOX molecules and the negatively charged silicon oxide pore walls, and self-association via π–π stacking interactions between DOX molecules.[43,44]

It has been reported that freshly etched porous Si (H-terminated) is a strong reducing agent that can react with molecular drugs such as DOX.[45] Therefore, UV-Vis spectroscopy and high-performance liquid chromatography-mass spectrometry (HPLC-MS) were performed to determine if the chemical composition and the structure of the DOX molecules loaded into the magnetic luminescent porous Si microparticles remain intact. The UV-Vis absorption spectrum of DOX extracted from the porous Si microparticles is identical with the DOX standard (Supporting Information, Figure S4). In addition, DOX extracted from the porous Si microparticles displays a single peak in the HPLC trace, with a retention time identical to that of the DOX standard (Figure 3a). Finally, mass spectrometry yields a spectrum identical to the DOX standard (Figure 3b), indicating that there is no significant chemical reaction between DOX and the porous Si matrix in the timescale and conditions of the present study. This lack of reactivity is attributed to the fact that the microparticles used in the present study are more extensively oxidized, presenting an inert SiO_2 surface to the DOX molecules (Supporting Information, Figure S1).

The DOX-loaded magnetic luminescent porous Si microparticles exhibit a continuous release at physiological pH and temperature; 90% of the adsorbed drug is released in 9 days (Figure 3c). Fluorescence microscope images indicate degradation of the porous Si matrix during the release period (Figure 3d), and no particles were observable by optical microscopy after day 9 under these release conditions. The degradation and dissolution process provides a mechanism by which the mesoporous drug carrier can be eliminated once it has performed its function, and this process can be monitored through the intrinsic luminescence of the porous Si matrix.

Free radical formation by means of cellular reduction of Fe (III) has been implicated in the observed cardiotoxicity of doxorubicin.[46] Cell viability assays were performed to determine if the iron oxide nanoparticles co-loaded with DOX increase the overall cytotoxicity of the formulation. HeLa (human cervical cancer) cells were incubated with free DOX together with iron oxide nanoparticles (using the same DOX:Fe_3O_4 ratio as that in the loaded porous Si microparticles) for 48 h, and the cell viability was evaluated by MTS (3-(4,5-dimethylthiazol-2-yl)-5-(3-carboxymethoxyphenyl)-2-(4-sulfophenyl)-2H-tetrazolium) assay. No significant difference in cytotoxicity was observed for the experiments with or without Fe_3O_4 nanoparticles (Supporting Information, Figure S5). This is attributed to the relatively small iron content in the microparticle formulations (Fe_3O_4:DOX mass ratio = 8:98).

The ability of the magnetic, luminescent porous Si microparticles to deliver DOX to HaLa cells *in vitro* under

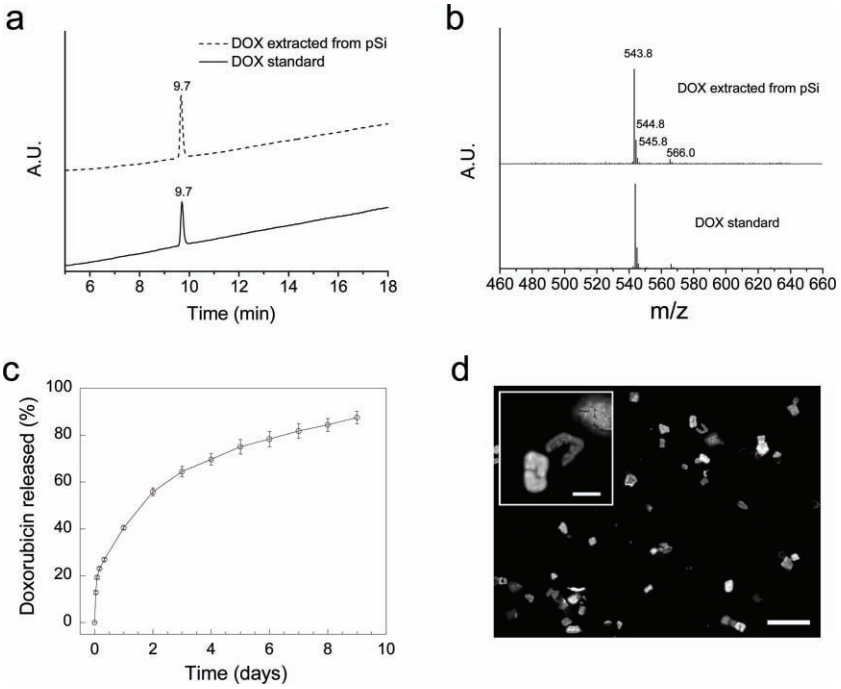

Figure 3. (a) HPLC analysis of DOX standard and DOX extracted from magnetic luminescent porous Si microparticles (UV-Vis detection wavelength at 480 nm). (b) Mass spectra of above samples separated by HPLC at retention time of 9.7 min. The signals at m/z 543.8 and 566.0 are $[DOX + H]^+$ and $[DOX + Na]^+$, respectively; the signals at m/z 544.8 and 545.8 correspond to the expected isotopic pattern for $[DOX + H]^+$. (c) Cumulative release of DOX from magnetic luminescent porous Si microparticles in aqueous PBS buffer solution (error bars indicate 1 S.D.). Data obtained from optical absorbance measurement (480 nm) of the supernatant. (d) Fluorescence microscope images of the microparticles after 6 days under release conditions (excitation wavelength 360 nm, emission filter bandpass 720 ± 80 nm). Scale bar is 100 μm (20 μm for the inset).

magnetic guidance was assessed. HeLa cells were seeded and cultured in a 60-mm Petri dish. A 0.10 mg quantity of DOX-loaded magnetic luminescent porous Si microparticles were added and attracted to one edge of the Petri dish using a rare earth permanent magnet. The Petri dish was agitated for 1 min with the magnet in place and then incubated for 24 h without agitation.

After incubation, the particles were still accumulated at the edge of the Petri dish in the vicinity of the magnet, and cell death was apparent in a small region (diameter ~1 cm) surrounding the particles (**Figure 4**a–d). Phase contrast microscope images obtained along a radius of the Petri dish, beginning at a spot 1 mm from the magnet location and ending at the center of the dish (Figure 4i), reveal the distance dependence of cell death. Few live cells, and a large quantity of light-refracting dead cells[47,48] are detected at the spot closest to the magnet, where the DOX-loaded microparticles are concentrated (Figure 4a). The ratio of live to dead cells increases further away from the edge where the microparticles are located, and the ratio increases dramatically at a distance >10 mm from the microparticles; the center of the dish contains what appears to be only live cells (Figure 4b–d). The phase contrast microscopy results are supported by fluorescence microscopy, using the fluorogenic viability stain calcein acetoxymethylester (Calcein AM), an intracellular esterase activity probe (Figure 4e–h).[49] The data indicate that the porous Si microparticles can deliver and release the drug doxorubicin to kill HeLa cells, and that the effect can be localized under the influence of an external magnetic field and reduce unintended systemic toxicity of the drug.

As a control, a Petri dish containing HeLa cells was incubated with the same quantity of DOX-loaded magnetic, luminescent porous Si microparticles, but in the absence of an applied magnetic field. A uniformly dispersed and relatively lower density of dead cells was observed in the Petri dish after 24 h incubation in this control experiment (Figure 4j and 4k). Similarly, HeLa cells incubated with 1 μg mL^{-1} of free DOX (equal to the quantity of DOX released from 0.10 mg of microparticles within 24 h) showed dispersed cell death throughout the Petri dish, consistent with the known cytotoxicity of the drug (Supporting Information, Figure S6). To verify the localized death of cells was not caused by the particles themselves, drug-free magnetic, luminescent porous Si microparticles were incubated with HeLa cells under the influence of a magnet. No dead cells were observed and the morphology of the cells remained normal (Supporting Information, Figure S7).

The effect of the quantity of particles on cell viability was also tested. A series of experiments employing 0.1, 0.2, and 0.4 mg of DOX-loaded microparticles were incubated in separate Petri dishes, each containing a similar quantity HeLa cells for 8 h under the influence of a magnetic field. The quantity of dead cells was observed to increase with increasing concentration of microparticles (Supporting Information, Figure S8).

3. Conclusions

In summary, microparticles containing both fluorescent and magnetic functions have been prepared by incorporating iron oxide nanoparticles into an intrinsically luminescent porous silicon matrix. A large quantity of doxorubicin (9.8% by mass) can be loaded into the composite microparticles, and a prolonged release of the drug is observed that is coincident with the physical degradation of the microparticulate carriers. Under the guidance of a magnetic field, *in vitro* localized delivery of the drug to cancer cells can be achieved, which provides a strategy to decrease the systemic toxicity of molecular drugs. Moreover, the low toxicity of the silicon and iron constituents of the composite microparticles, and the ability to load very dissimilar payloads into the porous Si matrix suggest that the approach may be of use for bioassay and therapeutic applications such as regional chemotherapy for the treatment of ovarian cancer through intraperitoneal administration.

NANO MICRO small

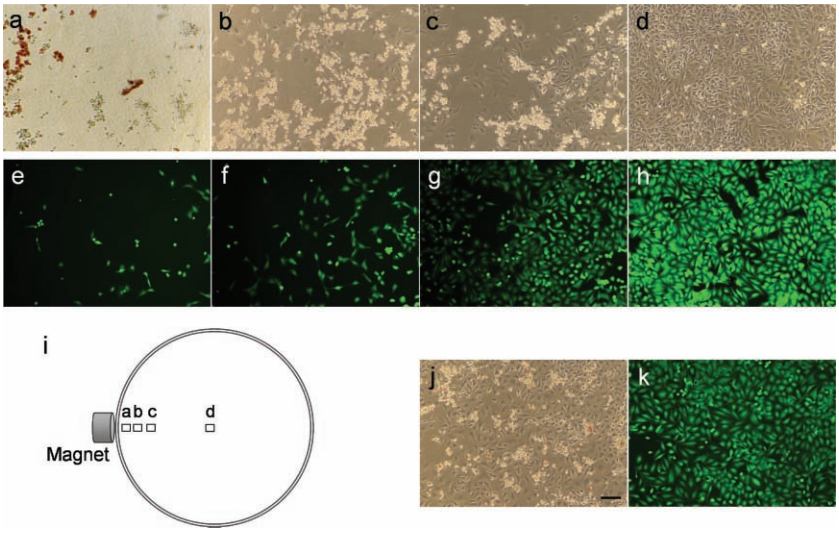

Figure 4. (a–d) Phase contrast microscope images of HeLa cells 24 h after incubation with DOX-loaded magnetic luminescent porous Si microparticles, showing magnetically guided delivery of doxorubicin. The position of each image relative to the external magnet is depicted in image (i). The microparticles were attracted to an edge of the Petri dish during incubation by means of a rare earth magnet placed external to the dish. (e–h) Fluorescence microscope images of HeLa cells stained with Calcein AM. Each image e-h is obtained at the approximate location as image a-d, respectively. (j, k) Phase contrast and fluorescence microscope images of a control dish of HeLa cells (24 h incubation with DOX-loaded magnetic luminescent porous Si microparticles) obtained without magnetic guidance. The image is representative of the entire dish, which shows no significant variation in cell morphology or fluorescence intensity as a function of position. Scale bar for all images is 100 μm.

Experimental Section

Preparation of Luminescent Porous Si Microparticles: Porous silicon samples were prepared by an anodic electrochemical etch of boron doped p-type Si wafers (0.0008–0.0012 Ω–cm resistivity, <100> orientation, Siltronix, inc.) in 3:1 (v:v) 48% aqueous HF:ethanol. A Teflon etch cell that exposed 8.8 cm^2 of the polished Si wafer surface was used. Samples were etched at a constant current density of 200 mA cm^{-2} for 150 s. The porous Si film was then removed from the crystalline Si substrate by application of a current pulse of 4 mA cm^{-2} for 250 s in a solution of 3.3% aqueous HF in ethanol. The free-standing porous Si film was immersed in a sodium borate buffer solution (6.2 mg mL^{-1}, pH = 9.2) for 5 min to activate the visible to near-IR emission, and it was then washed with deionized water several times. The luminescent porous Si film was placed in deionized water and fractured into microparticles by ultrasonication for 5 h (FS5, Fisher Scientific). The small fragments were removed by filtration through a 5 μm filter membrane (Millipore).

Preparation of Magnetic, Luminescent Porous Si Microparticles: Superparamagnetic iron oxide (Fe_3O_4) nanoparticles were synthesized following a published method.[40] The iron oxide nanoparticle suspension was diluted with 3 parts acetone to 1 part nanoparticle suspension in order to make the final concentration of iron oxide ~0.6 mg mL^{-1}. The luminescent porous Si microparticles were then added to the iron oxide nanoparticle suspension and stirred for 5 min in air at room temperature. The particulate product was isolated from solution by centrifugation and rinsed several times with acetone and water to remove the free iron oxide nanoparticles. The porous Si/iron oxide composite was then thermally oxidized and dehydrated in air at 100 °C overnight to further trap the iron oxide nanoparticles in the porous Si matrix.

Characterization: Scanning electron microscope (SEM) images were obtained using a Philips XL30 field emission ESEM operating in secondary electron emission mode. N_2 adsorption isotherms (interpreted with the BET and BJH models)[50] were measured on a Micromeritics ASAP2020 analyzer. The photoluminescence spectra were obtained using a Princeton Instruments/Acton spectrometer fitted with a liquid nitrogen-cooled silicon charge-coupled device detector (λ_{ex} = 370 nm and 460 nm longpass emission filter). The size of the iron oxide nanoparticles was characterized by transmission electron microscopy (2000EX, JEOL) and by dynamic light scattering (DLS) (Zetasizer Nano ZS90, Malvern Instruments). Magnetization data were collected using a Quantum Design MPMS2 SQUID magnetometer operating at 298 K. To quantify the amount of iron oxide contained in the composite particles, they were dissolved in hydrofluoric acid and the iron concentration of the solution was measured by atomic emission using an inductively coupled plasma instrument fitted with an optical emission spectrometer (ICP-OES, Optima 3000DV, Perkin Elmer).

Drug loading and release: Doxorubicin (DOX) was loaded into the magnetite-containing porous Si microparticles by mixing 1 mg of particles with 0.5 mL of an aqueous solution that was 1 mg mL^{-1} in DOX for 1 h in air at room termperature. The particles were harvested from the solution using a permanent rare earth magnet and rinsed 5 times with water to remove free DOX. The amount of DOX incorporated into the microparticles was determined by extracting the drug into a 1:1 water:ethanol solution 0.5 M in HCl and comparing the optical absorbance with a standard curve (λ = 480 nm, SpectraMax Plus 384, Molecular Devices). HPLC-MS was used to compare the structure of DOX extracted from porous Si microparticles (by ethanol) and DOX standard. A Thermo LCQdeca mass spectrometer coupled with an HP1100 LC system was employed for LC-UV-MS analysis. Electrospray ionization (ESI) was used and operated under positive ion mode. The UV detection wavelength was set to monitor 480 nm. A Shiseido C-18 column (MGIII, 2.0 mm ID × 50 mm) was used for separation with a flow rate of 0.20 ml min^{-1}. LC mobile phase A consisted of 5% methanol in water with 0.1% formic acid, and LC mobile phase B consisted of pure methanol with 0.1% formic acid. The LC gradient started from 20% B and was increased to 95% B in 18 min, then reduced to 20% B in 2 min, and then held at 20% B for 3 min. An Xcalibur 1.2 system was used for data acquisition and processing. The release of adsorbed DOX into aqueous buffer solution was studied by incubating 0.2 mg of DOX-loaded magnetic, luminescent porous Si microparticles in 1 mL of phosphate buffered saline (PBS) at 37 °C, with the solution replaced daily. At each time point, the particles were isolated from the aqueous phase by centrifugation, and the optical absorbance of the supernatant was measured to determine the amount of released DOX. Because DOX is moderately unstable

under physiological conditions,[45,51,52] the stability and degradation profile of free DOX in PBS under the above release conditions was determined by monitoring its optical absorbance. The drug release data were corrected using the degradation profile at each time point. Fluorescence microscopy images of the DOX-loaded microparticles were acquired using a fluorescence microscope (Eclipse LV150, Nikon) fitted with a thermoelectrically cooled CCD camera (CoolSNAP HQ^2, Photometrics), using an excitation wavelength of 360 nm and an emission filter with a bandpass at 720 ± 80 nm.

Localized delivery of DOX to HeLa cells: HeLa cells were seeded into 60-mm Petri dishes with 4 mL of cell media and cultured for 2 days (the cell confluency was ~90%). The DOX-loaded magnetic luminescent porous Si microparticles (0.1 mg to 0.4 mg, depending on the experiment) were then added and attracted to an edge of the Petri dish with a rare-earth permanent magnet. The Petri dish was agitated for 1 min with the magnet attached and then incubated at 37 °C for 8 or 24 hours without any agitation. A comparison of non-guided DOX delivery was conducted by incubating 0.1 mg of DOX-loaded magnetic luminescent porous Si microparticles with HeLa cells using the procedure described above but without the use of a magnet. Cell viability was examined by observing morphology of the cells using a phase contrast microscope (TE 300, Nikon) and by a fluorescent viability stain assay (Calcein AM, Invitrogen, Inc.).

Supporting Information

Supporting Information is available from the Wiley Online Library or from the author.

Acknowledgements

This work was supported by the National Cancer Institute of the National Institutes of Health through grant numbers U54 CA 119335 (UCSD CCNE), 5-R01-CA124427 (BRP), and U54 CA119349 (MIT CCNE) and by the National Science Foundation under Grant No. DMR-0806859. M.J.S., and E.R. are members of the Moores UCSD Cancer Center and the UCSD NanoTUMOR Center under which this work was conducted and supported by the NIH/NCI grant. J.P. thanks the Korea Science and Engineering Foundation (KOSEF) for a Graduate Study Abroad Scholarship. The authors thank Dr. Zhenqiang Wang and Prof. Seth M. Cohen for assistance with N_2 adsorption isotherm measurements, and Dr. Yongxuan Su and Prof. Kimberly Prather for assistance with HPLC-MS measurements.

[1] T. R. Sathe, A. Agrawal, S. Nie, *Anal. Chem.* **2006**, *78*, 5627
[2] N. Insin, J. B. Tracy, H. Lee, J. P. Zimmer, R. M. Westervelt, M. G. Bawendi, *ACS Nano* **2008**, *2*, 197.
[3] B. Zebli, A. S. Susha, G. B. Sukhorukov, A. L. Rogach, W. J. Parak, *Langmuir* **2005**, *21*, 4262.
[4] S. K. Mandal, N. Lequeux, B. Rotenberg, M. Tramier, J. Fattaccioli, J. Bibette, B. Dubertret, *Langmuir* **2005**, *21*, 4175.
[5] C. H. Yang, K. S. Huang, Y. S. Lin, K. Lu, C. C. Tzeng, E. C. Wang, C. H. Lin, W. Y. Hsu, J. Y. Chang, *Lab Chip* **2009**, *9*, 961.
[6] S. A. Corr, Y. P. Rakovich, Y. K. Gun'ko, *Nanoscale Res. Lett.* **2008**, *3*, 87.
[7] P. F. Zhang, H. J. Dou, W. W. Li, K. Tao, B. Xing, K. Sun, *Chem. Lett.* **2007**, *36*, 1458.
[8] S. P. Mulvaney, H. M. Mattoussi, L. J. Whitman, *Biotechniques* **2004**, *36*, 602.
[9] R. Wilson, D. G. Spiller, I. A. Prior, R. Bhatt, A. Hutchinson, *J. Mater. Chem.* **2007**, *17*, 4400.
[10] D. Pappas, K. Wang, *Anal. Chim. Acta* **2007**, *601*, 26.
[11] S. Dubus, J. F. Gravel, B. Le Drogoff, P. Nobert, T. Veres, D. Boudreau, *Anal. Chem.* **2006**, *78*, 4457.
[12] Y. C. Cao, Z. L. Huang, T. C. Liu, H. Q. Wang, X. X. Zhu, Z. Wang, Y. D. Zhao, M. X. Liu, Q. M. Luo, *Anal. Biochem.* **2006**, *351*, 193.
[13] D. Muller-Schulte, T. Schmitz-Rode, P. Borm, *J. Magn. Magn. Mater.* **2005**, *293*, 135.
[14] P. S. Eastman, W. M. Ruan, M. Doctolero, R. Nuttall, G. De Feo, J. S. Park, J. S. F. Chu, P. Cooke, J. W. Gray, S. Li, F. Q. F. Chen, *Nano Lett.* **2006**, *6*, 1059.
[15] J. N. Anker, Y. E. Koo, R. Kopelman, *Sens. Actuat. B-Chem.* **2007**, *121*, 83.
[16] M. Ettenauer, T. Posnicek, M. Brandl, V. Weber, D. Falkenhagen, *Biomacromolecules* **2007**, *8*, 3693.
[17] A. Quarta, R. Di Corato, L. Manna, A. Ragusa, T. Pellegrino, *IEEE Trans. Nanobio.* **2007**, *6*, 298.
[18] Q. Ma, C. Wang, X. G. Su, *J. Nanosci. Nanotech.* **2008**, *8*, 1138.
[19] J. Guo, W. L. Yang, Y. H. Deng, C. C. Wang, S. K. Fu, *Small* **2005**, *1*, 737.
[20] W. C. W. Chan, S. Nie, *Science* **1998**, *281*, 2016.
[21] B. Dubertret, P. Skourides, D. J. Norris, V. Noireaux, A. H. Brivanlou, A. Libchaber, *Science* **2002**, *298*, 1759.
[22] A. M. Derfus, W. C. W. Chan, S. N. Bhatia, *Adv. Mater.* **2004**, *16*, 961.
[23] S. Bauer, J. Park, J. Faltenbacher, S. Berger, K. von der Mark, P. Schmuki, *Integr. Biol.* **2009**, *1*, 525.
[24] Z. F. Li, E. Ruskenstein, *Nano Lett.* **2004**, *4*, 1463.
[25] J. H. Warner, A. Hoshino, K. Yamamoto, R. D. Tilley, *Angew. Chem. Int. Ed.* **2005**, *44*, 4550.
[26] L. Mangolini, U. Kortshagen, *Adv. Mater.* **2007**, *19*, 2513.
[27] J.-H. Park, L. Gu, G. v. Maltzahn, E. Ruoslahti, S. N. Bhatia, M. J. Sailor, *Nature Mater.* **2009**, *8*, 331.
[28] F. Erogbogbo, K. T. Yong, I. Roy, G. X. Xu, P. N. Prasad, M. T. Swihart, *ACS Nano* **2008**, *2*, 873.
[29] L. Wang, V. Reipa, J. Blasic, *Bioconjugate Chem.* **2004**, *15*, 409.
[30] W. Mertz, *Science* **1981**, *213*, 1332.
[31] Y. C. Yoo, S. K. Lee, J. Y. Yang, S. W. In, K. W. Kima, K. H. Chung, M. G. Chung, S. Y. Choung, *J. Health Sci.* **2002**, *48*, 186.
[32] S. C. Bayliss, R. Heald, D. I. Fletcher, L. D. Buckberry, *Adv. Mater.* **1999**, *11*, 318.
[33] L. T. Canham, *Adv. Mater.* **1995**, *7*, 1033.
[34] J. R. Dorvee, A. M. Derfus, S. N. Bhatia, M. J. Sailor, *Nature Mater.* **2004**, *3*, 896.
[35] E. Tasciotti, X. W. Liu, R. Bhavane, K. Plant, A. D. Leonard, B. K. Price, M. M. C. Cheng, P. Decuzzi, J. M. Tour, F. Robertson, M. Ferrari, *Nature Nano.* **2008**, *3*, 151.
[36] V. S. Y. Lin, K. Motesharei, K. P. S. Dancil, M. J. Sailor, M. R. Ghadiri, *Science* **1997**, *278*, 840.
[37] J. Salonen, A. M. Kaukonen, J. Hirvonen, V.-P. Lehto, *J. Pharm. Sci.* **2008**, *97*, 632.
[38] S. Godefroo, M. Hayne, M. Jivanescu, A. Stesmans, M. Zacharias, O. I. Lebedev, G. Van Tendeloo, V. V. Moshchalkov, *Nature Nano.* **2008**, *3*, 174.
[39] W. L. Wilson, P. F. Szajowski, L. E. Brus, *Science* **1993**, *262*, 1242.

[40] P. Berger, N. B. Adelman, K. J. Beckman, D. J. Campbell, A. B. Ellis, G. C. Lisensky, *J. Chem. Educ.* **1999**, *76*, 943.
[41] J.-H. Park, A. M. Derfus, E. Segal, K. S. Vecchio, S. N. Bhatia, M. J. Sailor, *J. Am. Chem. Soc.* **2006**, *128* 7938.
[42] M. V. Wolkin, J. Jorne, P. M. Fauchet, G. Allan, C. Delerue, *Phys. Rev. Lett.* **1999**, *82*, 197.
[43] M. Prokopowicz, A. Przyjazny, *J. Microencapsul.* **2007**, *24*, 694.
[44] S. Eksborg, *J. Pharm. Sci.* **1978**, *67*, 782.
[45] E. C. Wu, J.-H. Park, J. Park, E. Segal, F. Cunin, M. J. Sailor, *ACS Nano* **2008**, *2*, 2401.
[46] G. Minotti, P. Menna, E. Salvatorelli, G. Cairo, L. Gianni, *Pharmacol. Rev.* **2004**, *56*, 185.
[47] A. C. Scuderi, G. M. Paladino, C. Marino, F. Trombetta, *Cornea* **2003**, *22*, 468.
[48] E. C. Alfonso, D. M. Albert, K. R. Kenyon, N. L. Robinson, L. Hanninen, D. J. Damico, *Cornea* **1990**, *9*, 55.
[49] X. M. Wang, P. I. Terasaki, G. W. Rankin, D. Chia, H. P. Zhong, S. Hardy, *Hum. Immunol.* **1993**, *37*, 264.
[50] S. J. Gregg, K. S. W. Sing, *Adsorption, Surface Area and Porosity*, Academic Press Inc., London **1982**.
[51] J. H. Beijnen, O. Vanderhouwen, W. J. M. Underberg, *Int. J. Pharmaceutics* **1986**, *32*, 123.
[52] M. D. Chavanpatil, A. Khdair, Y. Patil, H. Handa, G. Mao, J. Panyam, *J. Pharm. Sci.* **2007**, *96*, 3379.

Received: May 18, 2010
Revised: July 27, 2010
Published online: